The Impact of Near-Surface Wind to Surface Current over a Coastal Region: A Numerical Example

H. Hsu[1] and Lie-Yauw Oey[2]

[1]National Center for Atmospheric Research
Boulder, CO
USA

[2]Princeton University
Princeton, NJ,
USA

1. Introduction

Wind stress and buoyancy flux are the two driving mechanisms to force the ocean waves and circulation. Both of them are directly connected to the lower atmosphere. Accurate predictions of ocean waves and circulation require accurate calculations of variables above the ocean surface. For coastal regions, additional considerations of coastal shape and topography are warranted. Therefore, high-resolution numerical models are the necessary tools. In this investigation, the impact of model resolutions to the near-surface wind field and its influence to the near-surface current over a coastal region are demonstrated. The model results are compared with wind-station time-series, Special Sensor Microwave/Imager (SSM/I) wind speeds, and the European Center for Medium Range Weather Forecast (ECMWF) reanalysis. Details of this effort can be found in Hsu *et al.* (2005). Furthermore, Dong and Oey (2005) describe the simulated coastal ocean circulations driven by the wind fields described here.

2. The Model and Experimental Design

As a demonstration, wind off the central and southern California coasts, including the Central California Shelf and Slope (CCSS), Southern California Bight (SoCB), and the transition zone in between - the Santa Barbara Channel (SBC) are simulated by different resolutions with the Coupled Ocean/Atmosphere Mesoscale Prediction System (COAMPS™). COAMPS solves the fully compressible, non-hydrostatic equations on Arakawa C-grid, and uses the height-based terrain following vertical coordinate. It includes physical parameterizations of short- and long-wave radiation (Harshvardhan *et al.* 1987), cumulus convection (Kain and Fritsch, 1990), and subgrid-scale boundary layer processes using a level-2.5 turbulent kinetic energy scheme (Therry and LaCarrere, 1983). Following Rutledge and Hobbs (1983), explicit moist physics contains prognostic equations of water vapor, cloud water, rain water, cloud ice and snowflakes. COAMPS has been extensively tested (Hodur 1997; Doyle, 1997; Thompson *et al.* 1997; Burk et al. 1999), and has been run operationally by the U.S. Navy in several coastal areas of the globe to provide real-time forecasts. COAMPS has nested-grid capability and uses MVOI (multivariate optimum interpolation) analysis to map the observations to its grid. Details can be found in Hodur (1997). COAMPS simulations require NOGAPS (Navy Operational Global Atmospheric Prediction System) outputs produced by FNMOC (Fleet Numerical Meteorology and Oceanography Center). The NOGAPS datasets with 1^{o} resolution are interpolated to the COAMPS domain grids as a first guess. The first guess fields are then further enhanced by available observations: radiosondes, surface stations and aircraft reports. Incremental assimilation that preserves mesoscale details is used every twelve hours to incorporate the observations.

The model topography is derived from the Defense Mapping Agency's *100-m* resolution dataset sub-sampled to *1-km* resolution, while sea surface temperature (SST) is obtained through an optimum interpolation analysis of FNMOC SST on each of the COAMPS domains. A triply nested domain is configured with one-way interaction between the outer domain (with horizontal grid size = Δ = *81 km*), the middle domain (Δ = *27 km*), and the inner domain (Δ = *9 km*) centered over the Santa Barbara Channel (Figure 1). The model top is *31 km* and there are *30* unevenly spaced vertical sigma levels, with *11* levels in the lowest *1.6 km*, down to *10 m* for the grid nearest the ocean surface. The Kain-Fritsch cumulus parameterization is used only on the two outer nests. The test period is March-May (1999) when the wind changes from its characteristics more typical of winter, to spring when multiple scales exist in the SBC.

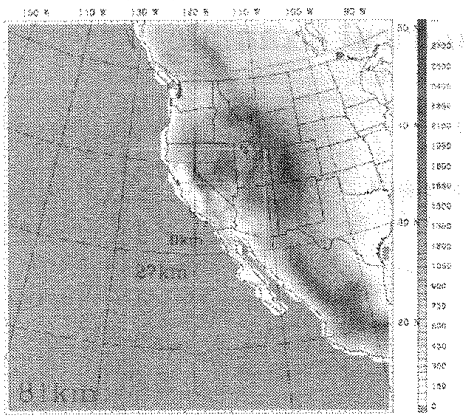

Figure 1. The triple-nest configurations of COAMPS used in the present study

3. The Near-Surface Wind Stress Curl

Ocean wind-driven circulation is strongly affected by the wind-stress curl. COAMPS-generated curl fields averaging over 3-month period (Mar-May/1999) for the inner and middle nests are shown in Fig. 2. For the inner nest (the upper panel), the wind stress curl maximizes downwind of Pt. Sur, Pt. Conception and western-most channel islands (San Miguel and Santa Rosa), with values $\approx$ *0.3-0.5 N m^{-2} per 100 km*, and $\approx$ *1 N m^{-2} per 100 km* south of Pt. Sur. Perlin et al. (2004) obtained similar values from a COAMPS (Δ = *9 km*) simulation off the Oregon-California coast (downwind of Cape Blanco; see their Fig.20). In the SBC, the wind maximizes near the channel's center resulting in a strong cyclonic curl in the northern two-thirds of the channel; in the southern third, the curl changes sign to become anticyclonic, though much weaker (c.f. observations by Dorman and Winant, 2000). The strong cyclonic curl in the channel is in part responsible for the spin-up of a cyclone in the ocean in the western portion of the channel, especially in spring (Oey, 1999; Munchow, 2000; Oey et al. 2004). On a larger scale, southward along the coast of the SoCB, the cyclonic wind stress curl continuously weakens, to less than *0.05 N m^{-2} per 100 km* at *32°N*. This equatorward weakening has been shown to be important forcing that in part determines the along-coast ocean currents (Oey, 1996, 1999).

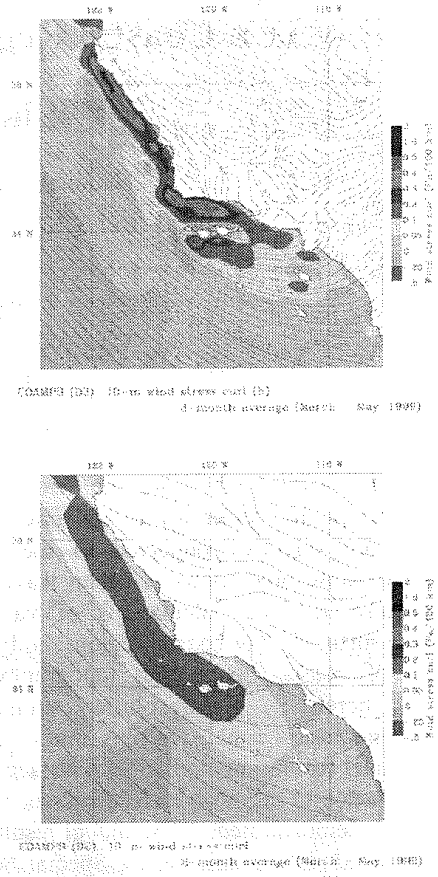

***Figure 2.** Contours of 3-month averaged (Mar-May/1999) COAMPS wind stress curl in the inner nest (Δ = 9 km) (upper panel) and in the middle nest (Δ =27 km) (lower panel) at the lowest sigma point (10 m over the ocean). Surface streamlines indicating flow directions are superimposed on each panel.*

By comparing middle and inner-nest fields we can check the effects of resolution. The middle-nest winds are smoother though speeds (not shown) do not differ much from inner nest. The large contrast is in wind stress curl (and divergence). The lower panel of Fig. 2 shows the averaged wind stress curl from the middle nest (Δ = *27 km*) which should be compared with the upper panel for the inner nest (Δ = *9 km*). Note the contrast in near-coast distributions and magnitudes. Largest wind stress curls in the middle-nest spread over *100 km* cross-shore, compared to the inner-nest distribution that has about half the scale and magnitudes that are *2~3* times more intense. Perlin et al. (2004) obtained similar results. They showed that wind stress curls calculated from QuikSCAT (Quick Scatterometer) satellite data and from the NCEP *32-km* hydrostatic Eta Model output gave values that are *3-5* times weaker than their inner nest COAMPS run. In QuikSCAT, near-coast ($\approx$ *50 km*) data had to be omitted. For Eta Model, the lower values were most likely a result of lower resolution. Below we will examine wind distributions from relatively dense arrays of observations which show maximum wind stress curls near the coast, with similar scales and strengths as the inner nest curls.

These results emphasize the importance of using good resolution especially near the coast.

4. Comparison with Observations and Reanalysis

We focus our comparison of model output against wind time-series at the wind stations in the vicinity of the SBC where largest discrepancies between model and observations are found. Because of the sharp bend in the coastline, flows in the SBC would entail small-scale dynamics that can be sensitive to grid resolution. We therefore also compare the inner and middle-nest solutions. In Fig. 3 the principal-axis (PA) winds observed (solid curves) at the six stations 46023 (B23), 46025 (B25), 46053 (B53), 46054 (B54), Santa Rosa (ROSA), and Island Gail (GAIL) are plotted. (B23, B25, B53, and B54 are NDBC buoy stations; ROSA and GAIL are MMS stations). The time-series comparison between the modeled and observed winds shows that the model does well in reproducing the observed fluctuations in March and April, but rather poorly in May. Of course, results from the inner nest compare better with the observations than those from the middle nest.

We extend the point-wise time-series comparison to yield information on spatial variability by comparing COAMPS and observed wind stress curl maps. The observed maps are derived by combining NDBC/coastal wind data with ECMWF and satellite products. The SSM/I (Special Sensor Microwave/Imager) data are produced as part of NASA's Pathfinder Program. A unified, physically based algorithm is used to simultaneously retrieve ocean wind speed (at 10 meters), water vapor, cloud water, and rain rate (Wentz, 1997; Wentz et al. 1998). Only the wind speed portion of the data is used for our purpose. Three-day averaged fields on $1/4^{o} \times 1/4^{o}$ grid were used. The original data already has a near-coast strip of width ≈ 50 *km* flagged, but further quality-check was found necessary to remove bad data at grid points where speeds and spatial gradients were unrealistically high.

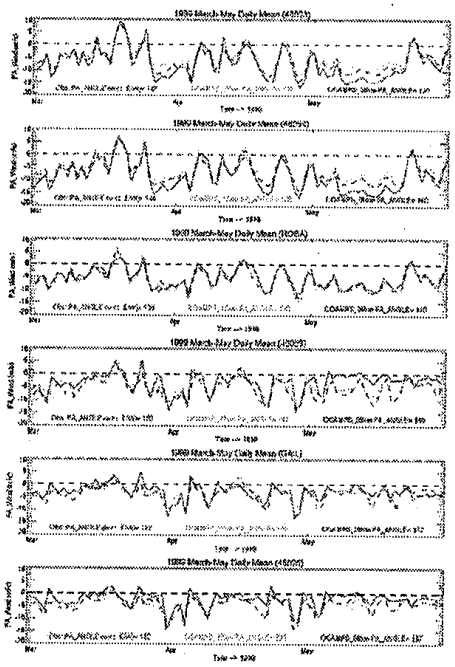

Figure 3. *Wind time series from March through May 1999, shown here as daily averaged principal-axis values at six NDBC and coastal stations arranged from north (top panel) to south: 46023, 46054, ROSA, 46053, GAIL and 46025. The principal-axis angles, measured in degrees anti-clockwise from true east, are printed in each panel. Solid curves are observed, dotted are modeled from the middle nest (Δ = 27 km), and dashed are modeled from the inner nest (Δ = 9 km).*

The data were then checked against the ECMWF reanalysis product on *1.125* ° Gaussian grid by computing the correlation between the two speed products over the period from 1992 through 1999. The correlation was found to be good (coefficients ≈ 0.8) over the open ocean, some *100 km* off the coast (not shown). There is also good agreement between SSM/I and offshore NDBC winds. The agreements between ECMWF u and v-winds and NDBC winds were also found to be excellent in the phasing, though the ECMWF speeds were too low within *100 km* of the coast. We therefore keep the ECMWF wind directions at off-shore locations but replace the speeds using the SSM/I data. The combined SSM/I and ECMWF product was then used with all available wind data to optimally interpolate onto Oey et al.'s (2001) ocean domain using *5 km* × *5 km* grid sizes at six-hourly interval from 1993-1999. This final product is referred to as the SEB – Satellite-ECMWF-Buoy dataset.

Figure 4 compares the ECMWF, COAMPS (Δ = *9 km*) and SEB wind stress curls averaged over March through May, 1999, focusing on the SBC and CCSS. In this small domain the ECMWF wind speed is weak in comparison to COAMPS and SEB. The ECMWF direction off CCSS is comparable to the higher-resolution COAMPS, but there is less onshore (or eastward) turning (than

COAMPS) in the SoCB. Note that away from the coast, SEB incorporates ECMWF wind directions into the optimum-interpolation analysis, and therefore also gives little turning in the SoCB. However, in the eastern portion of the SBC where the SEB analysis is dominated by observations the ECMWF wind also shows less turning than both COAMPS and SEB. The ECMWF wind stress curl is also weaker than COAMPS and SEB especially near the coast where values of about *0.5 Pa* per *100 km* may be seen in COAMPS and SEB results. The ECMWF wind field is actually very similar to the COAMPS field from the outer grid (Δ = *81 km*; not shown). Clearly, the ECMWF (or the coarse-grid COAMPS) wind is inadequate for use in ocean simulation in the CCSS-SBC-SoCB region (Dong and Oey, 2005).

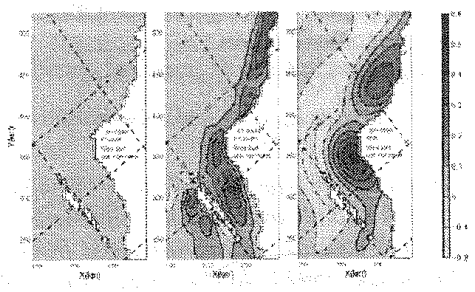

Figure 4. *Lower panel: three-month mean contours of the wind stress curl for ECMWF (left), COAMPS (middle), and SEB (right). The contour interval is 0.2 Pa/100km. The domain is enlarged focusing on the SBC and CCSS, and tilted 52° anticlockwise from north. Dashed dark lines are latitudes and longitudes in the indicated degrees.*

Both COAMPS and SEB give similar wind speeds, th ugh COAMPS is somewhat stronger offshore. SEB also shows a maximum speed just west of the channel while the COAMPS maximum is located further downwind south of the Channel Islands. The most important difference, however, is in the spatial distribution of the wind stress curl. In the channel, the SEB strong curl is concentrated in the western portion, while for COAMPS the region of strong curl extends further eastward. The SEB also shows a localized wind stress curl maximum immediately downwind of Pt. Buchon, while the COAMPS wind stress curl (again) shows a more coherent along-coast structure. Dong and Oey (2005) detail that the coastal ocean currents are sensitive to these subtle differences in the wind stress curl.

5. The Forced Ocean Circulation

The near-surface circulations over the SBC and Santa Maria Basin (SMB) were simulated by the Princeton Oceanic Model (Mellor, 2002). The model is configured into a 300 km × 500 km region with a resolution of 5 km to cover this region. The wind fields of ECMWF, COAMPS (Δ = *9 km*) and SEB are sampled into this grid-net to force the wind-driven circulations (Dong and Oey, 2005). Figures 5 and 6 show the mean near-surface currents (at z = -5 m) and sea surface height (SSH), respectively.

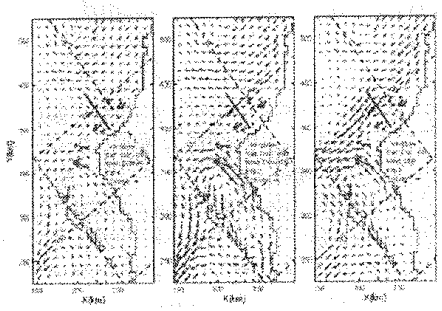

Figure 5. *The three-month mean currents at $z = -5m$ for wind-only experiments: ECMWF (left), COAMPS (middle), and SEB (right). The heavy-solid vectors are the observed mean currents (also at $z = -5m$) at the 12 mooring stations.*

The mean (or analysis period) is taken as the average over the period from 10 March to 31 May, thus excluding a 10-day (1–10 March) initial adjustment of the model dynamics to wind. Superimposed on the model current maps are also mean observed currents (heavy vectors; also at z = -5 m) for the same period. Fig. 5 show two primary circulation features: a southward flow in the SMB and cyclonic circulation in the western part of the SBC. The nearshore upwelling in the SMB and the upwelling in the cyclonic circulation in the western SBC show up as lows in the SSH contours in Fig. 6. It is clear that currents driven by the ECMWF wind are weaker than those driven by the COAMPS wind or the SEB wind. The ECMWF wind is the weakest among the three and i s resolution near the coast is not sufficient to resolve small-scale wind structures. In the experiment using the SEB wind, there are two localized upwelling centers: one off Point Buchon and the other, stronger one off Point Conception (Fig. 5c). These correspond to the two local maxima in the wind stress curl seen in Fig. 4c. By contrast, the other 2 experiments show only one upwelling center in the SBC. In the experiment using the ECMWF wind (Fig. 5a), the upwelling is weak (Fig. 6a), and the upwelling is strong and extends farther east into the channel in the experiment using the COAMPS wind (Fig. 6b). In the SMB, the mean near-surface currents driven by both ECMWF and COAMPS veer offshore near 35°N, whereas currents driven by the SEB wind are more intense and more aligned with the coast. This alongshore alignment of the currents in the SMB agrees better with the observed currents (Fig. 5c).

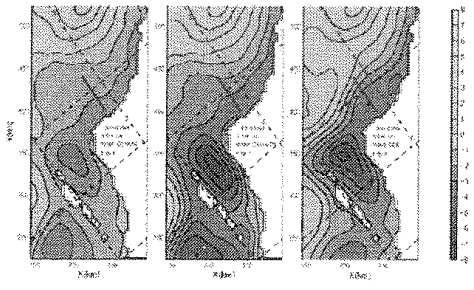

Figure 6. The three-month mean sea surface elevation for wind-only experiments: : ECMWF (left), COAMPS (middle), and SEB (right). The contour interval is 1cm.

6. Summary

Accurate wind information is necessary to simulate ocean currents. Both wind stress and wind stress curl in part, determine the internal pressure distribution of the ocean. This paper applies a regional atmospheric model, COAMPS, at moderately high resolution ($\Delta = 9$ *km*) to simulate winds off the central and southern California coast, the SBC in particular. Then, the simulated winds are used in ocean hindcast experiments. Here we check COAMPS against observations for the period March-May 1999. This is a spring transition period when the wind changes from its characteristics more typical of winter with storm passages in early March, through April and May when there exist more persistent and intense equatorward winds off central California coast and weak winds in the eastern portion of the SBC and also in the SoCB. The complexity of the wind field poses a challenge to any model.

We compare COAMPS with wind time-series from ocean and land stations. The agreements are good during March and April, but poor in May especially for stations in the eastern SBC. At the highest resolution used here ($\Delta = 9$ *km*), the model still fails to accurately simulate wind dynamics in the channel. The modeled winds east and west of the SBC are part of the same large-scale system over the open ocean, rather than uncorrelated as observed. On the other hand, the results from $\Delta = 9$ *km* are better than those from $\Delta = 27$ *km*, which suggests improved model skill with further grid-refinement incorporating high-resolution topography.

COAMPS results (at $\Delta = 9$ *km*) also show flow expansions behind coastal promontories (capes) and enhanced wind stress curls near coast. However, the along-coast curl field is again more coherent than observation. Results from the $\Delta = 9$ *km* grid compare better with observations than the $\Delta = 27$ *km* grid, and suggest that an even higher resolution incorporating fine topography is required. On a larger scale, COAMPS wind speeds over the open ocean are in fair agreements with those obtained from satellite (SSM/I). Over the SoCB, COAMPS correctly simulates onshore cyclonic turning of the wind in agreement with observation. This is in contrast to coarser-grid ECMWF reanalysis wind (on 1.125° Gaussian grid) and also to the outer-nest ($\Delta = 81$ *km*) COAMPS wind, both of which give little turning.

The near-surface circulation is sensitive to forcing by three different wind datasets: the ECMWF reanalysis wind; the COAMPS wind; and SEB, a wind product that we have derived using satellite SSM/I, ECMWF, and coastal buoy data. The ECMWF wind has coarse resolution (≈ 110 km) and is not suitable for circulation modeling in a coastal region that has significant wind stress and wind stress curl. The resulting modeled currents are weak and are different from observations. Both COAMPS and SEB winds generally produce more energetic currents. In particular, the cyclonic circulation in the western SBC is reproduced well. Subtle differences exist, however, between the two winds, especially in the corresponding wind stress curls. Well-organized local maxima in wind stress curls exist behind capes in the SEB dataset, whereas COAMPS shows a series of cellular wind stress curl patterns along the coast.

REFERENCES

Burk, S.D., T. Haack, and R.M. Samelson, 1999: Mesoscale simulation of supercritical, subcritical, and transcritical flow along coastal topography. *J. Atmos. Sci.*, **56**, 2780—2795.

Dong, C., and L.-Y. Oey, 2005: Sensitivity of coastal currents near Pt. Conception to forcing by three different winds: ECMWF, COAMPS and blended SSM/I-ECMWF-Buoy winds. *J. Phys. Oceanogr* ., 35, 1229-1244.

Dorman, C.E., and C.D. Winant, 2000: The structure and variability of the marine atmosphere around the Santa Barbara Channel. *Mon. Wea. Rev.*, **128,** 261—282.

Doyle, J.D., 1997: The influence of mesoscale topography on a coastal jet and rainband. *Mon. Wea. Rev.*, **125,** 1465—1488.

Hodur, R., 1997: The Naval Research Laboratory's Coupled Ocean/Atmosphere Mesoscale Prediction System (COAMPS). *Mon. Wea. Rev.*, **125,** 1414—1430.

Harshvardhan, D. Randall, and T. Corsetti, 1987: A fast radiation parameterization for atmospheric circulation models. *J. Geophys. Res.*, **92,** 1009—1016.

Hsu, H., L.-Y. Oey, W. Johnson, C. Dorman, and R. Hodur, 2005: Model wind in the central and southern California coastal zone. *(Submitted)*

Kain, J.S., and J.M. Fritsch, 1990: A one—dimensional entraining/detraining plume model and its application in convective parameterization. *J. Atmos. Sci.*, 47, 2784—2802.

Mellor, G. L., 2002: *Users Guide for a Three-Dimensional, Primitive Equation, Numerical Ocean Model.* Program in Atmospheric and Oceanic Sciences, Princeton University, 2003, 53 pp.

Munchow, A., 2000: Wind stress curl forcing of the coastal ocean near Point Conception, California. *J. Phys. Oceanogr.*, **30**, 1265-1280.

Oey, L.-Y., 1996: Flow around a coastal bend: a model of the Santa Barbara Channel eddy. *JGROceans*, 101, 16,667-16,682.

Oey, L.-Y., 1999. A Forcing Mechanism for the Poleward Flow off the Southern California Coast, *JGR-Oceans*, **104**, 13529-13539.

Oey, L.-Y., D.-P. Wang, T. Hayward, C. Winant, and M. Hendershott. 2001: Upwelling and cyclonic regimes of the near-surface circulation in the Santa Barbara Channel. *JGROceans*, **106**, 9213-9222.

Oey, L.-Y., C. Winant, E. Dever, W. Johnson, and D.-P. Wang, 2004: A model of the nearsurface circulation of the Santa Barbara Channel: comparison with observations and dynamical interpretations. *J. Phys. Oceanogr.*, **34**, 23-43.

Perlin, N., R.M. Samelson, and D.B. Chelton, 2004: Scatterometer and model wind and wind stress in the Oregon-northern California coastal zone. *Mon. Wea. Rev.*, **132**, 2110-2129.

Rutledge, S. A., and P.V. Hobbs, 1983: The mesoscale and microscale structure of organization of clouds and precipitation in midlatitude cyclones. VIII: A model for the "seeder—feeder" process in warm—frontal rainbands. *J. Atmos. Sci.*, **40**, 1185—1206.

Therry, G., and P. LaCarrere, 1983: Improving the eddy kinetic energy model for planetary boundary layer description. *Bound.—Layer Meteor.*, **25**, 63—88.

Thompson, W.T., S.D. Burk, and J. Rosenthal, 1997: An investigation of the Catalina eddy. *Mon. Wea. Rev.*, **125**, 1135—1146.

Wentz, F.J., 1997: A well-calibrated ocean algorithm for SSM/I", *J. Geophys. Res.*, **102**, C4, 8703-8718.

Wentz, F.J., and R.W. Spencer, 1998: SSM/I rain retrievals within a unified all-weather ocean algorithm, *J. Atmos. Sci.*, **55**, 1613-1627.